Geophysical Journal International

Geophys. J. Int. (2014) **197,** 1250–1267
Advance Access publication 2014 March 26

doi: 10.1093/gji/ggu077

An efficient finite-difference method with high-order accuracy in both time and space domains for modelling scalar-wave propagation

Sirui Tan and Lianjie Huang

Los Alamos National Laboratory, Geophysics Group, Los Alamos, NM 87545, *USA. E-mail: ljh@lanl.gov*

Accepted 2014 February 27. Received 2014 February 21; in original form 2013 July 30

SUMMARY

For modelling large-scale 3-D scalar-wave propagation, the finite-difference (FD) method with high-order accuracy in space but second-order accuracy in time is widely used because of its relatively low requirements of computer memory. We develop a novel staggered-grid (SG) FD method with high-order accuracy not only in space, but also in time, for solving 2- and 3-D scalar-wave equations. We determine the coefficients of the FD operator in the joint time-space domain to achieve high-order accuracy in time while preserving high-order accuracy in space. Our new FD scheme is based on a stencil that contains a few more grid points than the standard stencil. It is $2M$-th-order accurate in space and fourth-order accurate in time when using $2M$ grid points along each axis and wavefields at one time step as the standard SGFD method. We validate the accuracy and efficiency of our new FD scheme using dispersion analysis and numerical modelling of scalar-wave propagation in 2- and 3-D complex models with a wide range of velocity contrasts. For media with a velocity contrast up to five, our new FD scheme is approximately two times more computationally efficient than the standard SGFD scheme with almost the same computer-memory requirement as the latter. Further numerical experiments demonstrate that our new FD scheme loses its advantages over the standard SGFD scheme if the velocity contrast is 10. However, for most large-scale geophysical applications, the velocity contrasts often range approximately from 1 to 3. Our new method is thus particularly useful for large-scale 3-D scalar-wave modelling and full-waveform inversion.

Key words: Numerical solutions; Numerical approximations and analysis; Computational seismology; Wave propagation.

1 INTRODUCTION

Large-scale seismic imaging and inversion requires an efficient and accurate algorithm for numerous simulations of forward and backward wave propagation, as required by reverse-time migration (e.g. Etgen *et al.* 2009) and full-waveform inversion (e.g. Virieux & Operto 2009). Various finite-difference (FD) methods have been developed for this purpose during the past decades. The staggered-grid (SG) FD method is widely used (Virieux 1984, 1986). It is naturally connected with the velocity-stress formulation of the wave equation, which allows convenient implementation of both pressure sources and displacement sources. The SGFD method has better stability for models with high velocity contrasts and generally is more accurate than conventional FD methods (e.g. Zingg 2000; Moczo *et al.* 2007). The idea of SGFD schemes traces back to a seminal paper by Yee (1966) for the simulation of electromagnetic waves. Virieux (1984, 1986) introduced the idea for modelling seismic-wave propagation.

Controlling both space and time dispersion errors is one of the biggest challenges for FD modelling of seismic-wave propagation. In a seismogram, the space dispersion error usually exists in the form of a phase lag, while the time dispersion error usually results in a phase lead. High-order approximations to the spatial derivatives have been developed to successfully control space dispersion errors. For example, Levander (1988) extended Virieux's scheme to fourth-order accuracy in space. Arbitrary even-order accuracy in space can be achieved by increasing the length of FD operators. The coefficients of the operators are usually determined using Taylor expansion (e.g. Fornberg 1998). Other methods have emerged to derive the coefficients of the FD operators using the optimization technique (Holberg 1987; Tam & Webb 1993), the scaled binomial windows (Chu & Stoffa 2012) and the low-rank approximation (Song *et al.* 2013).

Although very high-order accuracy has been achieved in space, second-order time discretization is popular because of its relatively low requirements of computer memory and its capability of preserving wave energy. In the following, we refer the scheme with $2M$-th-order accuracy in space and second-order accuracy in time as the standard SGFD scheme, and denote it by $(2M, 2)$. For the standard SGFD scheme,

one often has to use a time interval as small as one-fourth to one-third of the maximum allowed time interval determined by stability conditions to control time dispersion errors during long-distance wave propagation.

To enhance the temporal order of accuracy without significantly increasing computer memory requirement, Dablain (1986) applied the Lax-Wendroff approach (Lax & Wendroff 1964) for modelling scalar-wave propagation. High-order temporal derivatives are replaced by spatial derivatives using the wave equation. In practice, Dablain (1986) demonstrated that it is sufficient to assume homogeneous media when converting the derivatives. Similar technique was developed by Blanch & Robertsson (1997) for modelling wave propagation in media described by Zener elements. Both methods mentioned above are up to fourth-order accurate in time and 10th-order accurate in space. For large-scale 3-D modelling, higher-order accuracy in space, for example, 16th-order, is sometimes preferable because a large grid spacing can be used to reduce the computer-memory requirements. It is not clear whether fourth-order accuracy in time is necessary or sufficient when combined with very high-order approximation in space. Moreover, the Lax-Wendroff approach involves expensive calculations of high-order spatial derivatives for 3-D modelling (e.g. Chen 2011).

Geller & Takeuchi (1995, 1998) developed optimally accurate FD schemes for modelling elastic-wave propagation. Their derivations yield implicit schemes which are solved by an explicit predictor-corrector algorithm (Geller & Takeuchi 1998; Takeuchi & Geller 2000). The predictor-corrector optimally accurate FD scheme is essentially equivalent to the Lax-Wendroff scheme with fourth-order accuracy in both space and time (Mizutani *et al.* 2000). The optimally accurate schemes have not yet been widely used in practical FD modelling. The unpopularity might result from the relatively complicated theory compared to the standard SGFD schemes and the lack of user-friendly codes (e.g. Moczo *et al.* 2007).

To reduce time dispersion errors, Liu & Sen (2009, 2011) derived FD schemes on both conventional and staggered grids using the Taylor expansion of dispersion relations in the joint time-space domain. They demonstrated that their schemes can reach $2M$-th-order accuracy both in space and time along eight wave propagation directions in 2-D and 48 directions in 3-D. However, the temporal accuracy is still second-order along other propagation directions. Recently, Liu & Sen (2013) developed a diamond-shaped stencil on conventional grids for 2-D modelling of scalar-wave propagation, and showed that their scheme can reach $2M$-th-order accuracy both in space and time along all propagation directions. The number of grid points in the diamond-shaped stencil is $\sim M^2$ for their $2M$-th-order scheme, as opposed to $\sim M$ in the standard stencil. The diamond-shaped stencil contains $\sim M^3$ grid points for 3-D modelling, which requires a large amount of floating-point operations and thus is very computationally expensive for large-scale 3-D modelling.

To achieve both accuracy and efficiency, we develop FD schemes in the time-space domain using new stencils with only a few more grid points than the standard stencil. The new scheme, denoted as ($2M$, 4) or ($2M$, 6), is $2M$-th-order accurate in space and fourth- or sixth-order accurate in time. Our new FD schemes preserve the advantages of the standard SGFD scheme in controlling space dispersion errors, while significantly increase the capability of suppressing time dispersion errors with only slightly larger stencils than the latter. Our new FD scheme ($2M$, 4) is similar to a Lax-Wendroff FD approach where the high-order derivatives are approximated using a special discretization scheme. However, our method is preferable to the Lax-Wendroff approach (Dablain 1986; Chen 2011) for the following reasons. First, to achieve given orders of accuracy in time and space, our schemes require a smaller amount of floating-point operations than the Lax-Wendroff schemes. Second, we derive analytical expressions of the FD coefficients for our new schemes with arbitrary even-order accuracy in space, while the FD coefficients for the Lax-Wendroff schemes with up to 10th-order accuracy in space are tabulated (Dablain 1986; Chen 2011). The first advantage of our new FD schemes is particularly important for efficient modelling of large-scale 3-D scalar-wave propagation.

We perform dispersion analysis for our new FD schemes with 16th-order accuracy in space and fourth- or sixth-order accuracy in time, and use the schemes to conduct numerical modelling of scalar-wave propagation in 2- and 3-D complex media. Our results demonstrate that the computational efficiency of our new FD scheme ($2M$, 4) is approximately two times higher than that of the standard SGFD scheme for a given 2- or 3-D modelling problem involving velocity contrasts up to five. Although our scheme ($2M$, 4) is fourth-order in time, we show that it is generally more efficient than the scheme ($2M$, 6) for complex media. This confirms that fourth-order accuracy in time is necessary and sufficient when combined with a high-order approximation of spatial derivatives in the wave equation.

This paper is organized as follows. We first derive our new FD schemes with $2M$-th-order accuracy in space and fourth- and sixth-order accuracy in time. This is followed by dispersion, stability and efficiency analyses. We then conduct numerical modelling of scalar-wave propagation in 2- and 3-D complex media with various velocity contrasts and compare the efficiency and accuracy of our new FD results with those obtained using the standard SGFD scheme.

2 EFFICIENT FD SCHEMES WITH $2M$-TH-ORDER ACCURACY IN SPACE AND FOURTH- OR SIXTH-ORDER ACCURACY IN TIME

The velocity-stress formulation of the scalar-wave equation is given by

$$\begin{aligned} \frac{\partial p}{\partial t} + K(\boldsymbol{x})\nabla \cdot \boldsymbol{v} &= 0, \\ \frac{\partial \boldsymbol{v}}{\partial t} + \frac{1}{\rho}\nabla p &= 0, \end{aligned} \tag{1}$$

where ρ is the constant density, $K(\boldsymbol{x})$ is the bulk modulus, $p(\boldsymbol{x}, t)$ is the pressure and $\boldsymbol{v}(\boldsymbol{x}, t) = (u(\boldsymbol{x}, t), v(\boldsymbol{x}, t), w(\boldsymbol{x}, t))^{\mathrm{T}}$ is the vector of the velocity wavefield. The spatial variable $\boldsymbol{x}$ is in 2- or 3-D. We develop efficient FD schemes with $2M$-th-order accuracy in space and fourth- or

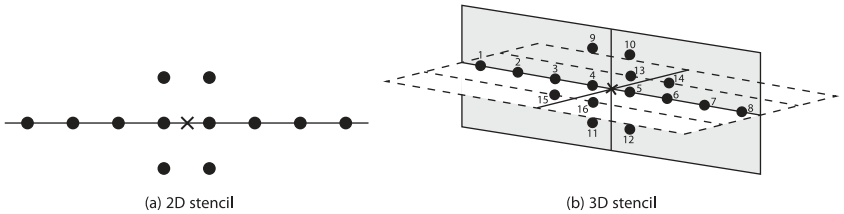

Figure 1. Illustration of the finite-difference stencils of our new FD scheme (2*M*, 4) when $2M = 8$ for (a) 2-D and (b) 3-D modelling. Grid points #1–12 in the shaded plane in (b) are the same as the 2-D case in (a), while grid points #13–16 in the perpendicular plane are added for the 3-D case.

sixth-order accuracy in time denoted by (2*M*, 4) or (2*M*, 6). Our new FD scheme (2*M*, 4) is based on the stencils depicted in Fig. 1. Compared with the stencil for the standard SG scheme, the new stencils contain a few additional grid points off the axis.

2.1 2-D modelling problems

The usual SGFD discretization of eq. (1) leads to

$$p_{0,0}^{j} = p_{0,0}^{j-1} - K_{0,0}\left(D_x^{2M,4}u_{0,0}^{j-1/2} + D_z^{2M,4}w_{0,0}^{j-1/2}\right)\Delta t,$$

$$u_{1/2,0}^{j+1/2} = u_{1/2,0}^{j-1/2} - \frac{1}{\rho}D_x^{2M,4}p_{1/2,0}^{j}\Delta t,$$

$$w_{0,1/2}^{j+1/2} = w_{0,1/2}^{j-1/2} - \frac{1}{\rho}D_z^{2M,4}p_{0,1/2}^{j}\Delta t, \tag{2}$$

where $D_x^{2M,4}$ and $D_z^{2M,4}$ are FD operators along x- and z-axis, respectively. The superscript (2*M*, 4) indicates that our scheme (2) has $2M$-th-order accuracy in space and fourth-order accuracy in time. Term $p_{m,n}^{j}$ represents the discretized pressure wavefield $p(x + mh, z + nh, j\Delta t)$ and $u_{m,n}^{j+1/2}$ and $w_{m,n}^{j+1/2}$ denote the discretized velocity wavefield. $K_{0,0}$ is the discretized bulk modulus at (x, z). For the case of constant density, eq. (2) becomes a discretized scalar-wave equation for pressure

$$\frac{p_{0,0}^{j+1} - 2p_{0,0}^{j} + p_{0,0}^{j-1}}{\Delta t^2} = c_{0,0}^2\left[\left(D_x^{2M,4}\right)^2 + \left(D_z^{2M,4}\right)^2\right]p_{0,0}^{j}, \tag{3}$$

where $c_{0,0} = \sqrt{\frac{K_{0,0}}{\rho}}$ is the wave speed, and (0, 0) stands for the spatial position (x, z).

At each time step, we define $D_x^{2M,4}$ on the stencil shown in Fig. 1(a) using

$$\frac{\partial p}{\partial x} \approx D_x^{2M,4}p_{0,0} = \frac{1}{h}\left[\sum_{m=1}^{M} d_{m,0}(p_{m-1/2,0} - p_{-m+1/2,0}) + d_{1,1}(p_{1/2,1} - p_{-1/2,1} + p_{1/2,-1} - p_{-1/2,-1})\right], \tag{4}$$

where h denotes the spatial grid spacing, and we omit the superscripts for denoting time steps without causing confusion. Similarly, we define $D_z^{2M,4}$ using

$$\frac{\partial p}{\partial z} \approx D_z^{2M,4}p_{0,0} = \frac{1}{h}\left[\sum_{m=1}^{M} d_{m,0}(p_{0,m-1/2} - p_{0,-m+1/2}) + d_{1,1}(p_{1,1/2} - p_{1,-1/2} + p_{-1,1/2} - p_{-1,-1/2})\right]. \tag{5}$$

We determine coefficients $d_{m,0}$ and $d_{1,1}$ using dispersion relations in the frequency-wavenumber domain. Fourier transforms of eqs (4) and (5) lead to

$$\mathrm{i}k_x \approx \frac{2\mathrm{i}}{h}\left[\sum_{m=1}^{M} d_{m,0}\sin((m-1/2)k_x h) + 2d_{1,1}\sin(k_x h/2)\cos(k_z h)\right], \tag{6}$$

$$\mathrm{i}k_z \approx \frac{2\mathrm{i}}{h}\left[\sum_{m=1}^{M} d_{m,0}\sin((m-1/2)k_z h) + 2d_{1,1}\sin(k_z h/2)\cos(k_x h)\right]. \tag{7}$$

Substituting eqs (6) and (7) in the Fourier transform of eq. (3), we obtain the truncation error

$$\varepsilon = \left[\sum_{m=1}^{M} d_{m,0}\sin((m-1/2)k_x h) + 2d_{1,1}\sin(k_x h/2)\cos(k_z h)\right]^2 + \left[\sum_{m=1}^{M} d_{m,0}\sin((m-1/2)k_z h) + 2d_{1,1}\sin(k_z h/2)\cos(k_x h)\right]^2$$
$$- \frac{1}{2r_{0,0}^2}\left[1 - \cos(r_{0,0}kh)\right], \tag{8}$$

where $k = \sqrt{k_x^2 + k_z^2}$ and

$r_{0,0} = c_{0,0}\Delta t / h$

is the local Courant-Friedrichs-Lewy (CFL) number. Taylor expansion of eq. (8) leads to

$$\varepsilon = \sum_{\xi=1}^{M} \sum_{\eta=\lceil \xi/2 \rceil}^{\xi} \beta_{\xi,\eta} k_x^{2\eta} k_z^{2(\xi-\eta)} h^{2\xi} + O(h^{2M+2}),$$

where $\lceil \xi/2 \rceil$ stands for the largest integer that is not greater than $\xi/2$, $\beta_{\xi,\eta}$ are polynomials of CFL number $r_{0,0}$, and coefficients $d_{m,0}$ and $d_{1,1}$. We design our new FD scheme to have $2M$-th-order accuracy in space and fourth-order accuracy in time, such that

$$\beta_{\xi,\xi} = 0, \quad \xi = 1, 2, \cdots, M,$$

$$\beta_{2,1} = 0.$$

Then we obtain a system of equations for coefficients $d_{m,0}$ and $d_{1,1}$ given by

$$\sum_{m=1}^{M} (2m-1)^{2\xi-1} d_{m,0} + 2d_{1,1} - r_{0,0}^{2\xi-2} = 0, \quad \xi = 1, 2, \cdots, M,$$

$$d_{1,1}\left[\sum_{m=1}^{M} (2m-1) d_{m,0} + 2d_{1,1}\right] - \frac{r_{0,0}^2}{24} = 0. \tag{9}$$

The solution of eq. (9) gives

$$d_{1,1} = \frac{r_{0,0}^2}{24},$$

$$d_{1,0} = 1 - 2d_{1,1} - \sum_{m=2}^{M} (2m-1)\, d_{m,0},$$

$$d_{m,0} = \frac{(-1)^{m+1}}{2m-1} \prod_{l=1, l\neq m}^{M} \frac{(2l-1)^2 - r_{0,0}^2}{|(2m-1)^2 - (2l-1)^2|}, \qquad m = 2, 3, \cdots, M.$$

Note that the FD coefficients $d_{m,0}$ and $d_{1,1}$ depend on $r_{0,0}$ and thus on the local wave speed $c_{0,0}$ for a given spatial grid spacing h and a time interval Δt. If we have $r_{0,0} \to 0$ or $\Delta t \to 0$, this limit case is exactly the standard SG scheme with coefficients (e.g. Liu & Sen 2011)

$$d_{1,1} \to 0, \quad \text{as } r_{0,0} \to 0,$$

$$d_{m,0} \to \frac{(-1)^{m+1}}{2m-1} \prod_{1\leq l\leq M, l\neq m} \frac{(2l-1)^2}{|(2l-1)^2 - (2m-1)^2|}, \qquad m = 1, \cdots, M, \quad \text{as } r_{0,0} \to 0.$$

The fact that $d_{1,1} = r_{0,0}^2/24 \neq 0$ in our new FD scheme indicates that including the grid points lying off the axis in the stencil is necessary to obtain fourth-order accuracy in time. The rotated-SG (or partially SG) FD scheme (e.g. Saenger *et al.* 2000) also involves approximation of the spatial derivatives using grid points lying off the axis. However, all components of velocity wavefields are located at the same grid position in the rotated-SGFD scheme, while each velocity component is defined at a different grid position in our scheme as the standard SGFD scheme.

In a heterogeneous medium, $c_{0,0}$ is determined according to the wave speed at each spatial grid point. For challenging cases with a large grid spacing and large velocity contrasts, the averaging strategy developed by Moczo *et al.* (2002) can be used to reduce errors caused by material heterogeneities.

Since the FD coefficients vary spatially in a heterogeneous medium, one may compute and store the coefficients in computer memory for each grid point before numerical modelling of wave propagation. However, a large amount of computer memory is needed to store these coefficients for large-scale 3-D modelling. Our implementation strategy is to compute and store the values of the FD coefficients for the wave speed values in a given model. For example, for a given model with the wave speed ranging from 1500 to 5000 m s^{-1}, we calculate and store the FD coefficients for wave speeds of 1500, 1501, $\cdots$, 5000 m s^{-1} with an increment of 1 m s^{-1}. Approximately only 0.1 MB of computer memory is needed to store the values of the FD coefficients using our new FD scheme with 16th-order accuracy in space. Therefore, our new FD scheme requires almost the same amount of computer memory as the standard SGFD scheme for large-scale 3-D modelling.

Similar to our new FD scheme, the Lax-Wendroff FD approach (e.g. Dablain 1986; Chen 2011) has fourth-order accuracy in time using wavefields at one time step to compute those at the next time step. In the Appendix, we demonstrate the relationship between our new FD scheme and a Lax-Wendroff FD approach where the high-order derivatives are approximated using a special discretization scheme. Compared with the Lax-Wendroff approach (Dablain 1986; Chen 2011), our FD scheme (A2) written in the form of the Lax-Wendroff formulation contains an additional term involving the fifth derivative for the 2-D case. A direct implementation of scheme (A2) requires calculation of

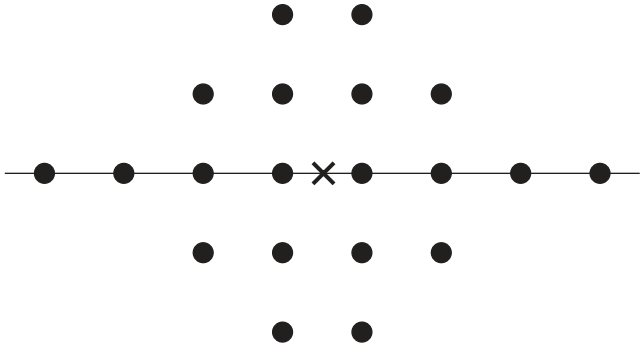

Figure 2. Illustration of the finite-difference stencil of our new FD scheme ($2M$, 6) when $2M = 8$ for 2-D modelling.

the derivatives in eq. (A3). Obviously, our new FD scheme (A5) requires a smaller amount of floating-point operations than the standard Lax-Wendroff FD scheme because the FD coefficients of each grid point in the stencil of our new FD scheme are combined. Therefore, our scheme is computationally more efficient than the standard Lax-Wendroff FD scheme for modelling of wave propagation in large-scale 3-D media.

In the following, we derive a new FD scheme ($2M$, 6) with $2M$-th-order accuracy in space and sixth-order accuracy in time on the stencil shown in Fig. 2. The FD operator is

$$\frac{\partial p}{\partial x} \approx D_x^{2M,6} p_{0,0} = \frac{1}{h}\Bigg[\sum_{m=1}^{M} a_{m,0}(p_{m-1/2,0} - p_{-m+1/2,0}) + a_{1,1}(p_{1/2,1} - p_{-1/2,1} + p_{1/2,-1} - p_{-1/2,-1}) + a_{2,1}(p_{3/2,1} - p_{-3/2,1} + p_{3/2,-1} - p_{-3/2,-1} + p_{1/2,2} - p_{-1/2,2} + p_{1/2,-2} - p_{-1/2,-2})\Bigg]. \tag{10}$$

The analytical expressions of the coefficients in eq. (10) are

$$a_{1,1} = \frac{r_{0,0}^2}{3840}\left(230 - 21r_{0,0}^2\right),$$

$$a_{2,1} = \frac{r_{0,0}^2}{3840}\left(-10 + 3r_{0,0}^2\right),$$

$$a_{1,0} = f_1 - 3a_{2,0},$$

$$a_{2,0} = \frac{f_2 - f_1}{24},$$

$$a_{m,0} = \frac{(-1)^{m+1}}{2m-1}\prod_{l=1,l\neq m}^{M}\frac{(2l-1)^2 - r_{0,0}^2}{|(2m-1)^2 - (2l-1)^2|}, \qquad m = 3, 4, \cdots, M,$$

where

$$f_1 = 1 - 2a_{1,1} - 8a_{2,1} - \sum_{m=3}^{M}(2m-1)a_{m,0},$$

$$f_2 = r_{0,0}^2 - 2a_{1,1} - 56a_{2,1} - \sum_{m=3}^{M}(2m-1)^3 a_{m,0}.$$

We compare the computational efficiency and accuracy of our FD schemes ($2M$, 4) and ($2M$, 6) in Section 2.3 to demonstrate which scheme is preferable.

2.2 3-D modelling problems

Extending our new FD schemes to 3-D modelling problems is straightforward. To derive our new 3-D FD scheme ($2M$, 4), we define the FD operators on the stencil shown in Fig. 1(b) when the spatial order of accuracy is $2M = 8$. There are 16 grid points in the stencil. Grid points #1–12 in the shaded plane in Fig. 1(b) are the same as Fig. 1(a) for the 2-D case, while grid points #13–16 in the perpendicular plane are added for the 3-D case.

The approximation to $\frac{\partial p}{\partial x}$ for our $(2M, 4)$ scheme is given by

$$\frac{\partial p}{\partial x} \approx D_x^{2M,4} p_{0,0,0} = \frac{1}{h}\sum_{m=1}^{M} d_{m,0,0}(p_{m-1/2,0,0} - p_{-m+1/2,0,0}) + \frac{1}{h} d_{1,1,0}(p_{1/2,1,0} - p_{-1/2,1,0} + p_{1/2,-1,0} - p_{-1/2,-1,0} + p_{1/2,0,1} - p_{-1/2,0,1} + p_{1/2,0,-1} - p_{-1/2,0,-1}), \tag{11}$$

where $p_{m,n,l} = p(x + mh, y + nh, z + lh)$ and thus $p_{0,0,0} = p(x, y, z)$. The coefficients in eq. (11) are

$$d_{1,1,0} = \frac{r_{0,0,0}^2}{24},$$

$$d_{1,0,0} = 1 - 4d_{1,1,0} - \sum_{m=2}^{M}(2m-1)d_{m,0,0},$$

$$d_{m,0,0} = \frac{(-1)^{m+1}}{2m-1}\prod_{l=1,l\neq m}^{M}\frac{(2l-1)^2 - r_{0,0,0}^2}{|(2m-1)^2 - (2l-1)^2|}, \qquad m = 2, 3, \cdots, M,$$

where

$$r_{0,0,0} = c_{0,0,0}\Delta t / h.$$

To achieve sixth-order accuracy in time, our new FD scheme $(2M, 6)$ uses the following approximation:

$$\begin{aligned}\frac{\partial p}{\partial x} \approx D_x^{2M,6} p_{0,0,0} = {} & \frac{1}{h}\sum_{m=1}^{M} a_{m,0,0}(p_{m-1/2,0,0} - p_{-m+1/2,0,0}) + \frac{1}{h} a_{1,1,0}(p_{1/2,1,0} - p_{-1/2,1,0} + p_{1/2,-1,0} - p_{-1/2,-1,0} \\ & + p_{1/2,0,1} - p_{-1/2,0,1} + p_{1/2,0,-1} - p_{-1/2,0,-1}) + \frac{1}{h} a_{2,1,0}(p_{3/2,1,0} - p_{-3/2,1,0} + p_{3/2,-1,0} - p_{-3/2,-1,0} \\ & + p_{3/2,0,1} - p_{-3/2,0,1} + p_{3/2,0,-1} - p_{-3/2,0,-1} + p_{1/2,2,0} - p_{-1/2,2,0} + p_{1/2,-2,0} - p_{-1/2,-2,0} + p_{1/2,0,2} - p_{-1/2,0,2} \\ & + p_{1/2,0,-2} - p_{-1/2,0,-2}) + \frac{1}{h} a_{1,1,1}(p_{1/2,1,1} - p_{-1/2,1,1} + p_{1/2,-1,1} - p_{-1/2,-1,1} + p_{1/2,1,-1} - p_{-1/2,1,-1} \\ & + p_{1/2,-1,-1} - p_{-1/2,-1,-1}).\end{aligned} \tag{12}$$

The coefficients in eq. (12) are

$$a_{1,1,0} = \frac{r_{0,0,0}^2}{3840}\left(230 - 29r_{0,0,0}^2\right),$$

$$a_{2,1,0} = \frac{r_{0,0,0}^2}{3840}\left(-10 + 3r_{0,0,0}^2\right),$$

$$a_{1,1,1} = \frac{r_{0,0,0}^4}{960},$$

$$a_{1,0,0} = f_3 - 3a_{2,0,0},$$

$$a_{2,0,0} = \frac{f_3 - f_4}{24},$$

$$a_{m,0,0} = \frac{(-1)^{m+1}}{2m-1}\prod_{l=1,l\neq m}^{M}\frac{(2l-1)^2 - r_{0,0,0}^2}{|(2m-1)^2 - (2l-1)^2|}, \qquad m = 3, 4, \cdots, M,$$

where

$$f_3 = 1 - 4a_{1,1,0} - 16a_{2,1,0} - 4a_{1,1,1} - \sum_{m=3}^{M}(2m-1)a_{m,0,0},$$

$$f_4 = r_{0,0,0}^2 - 4a_{1,1,0} - 112a_{2,1,0} - 4a_{1,1,1} - \sum_{m=3}^{M}(2m-1)^3 a_{m,0,0}.$$

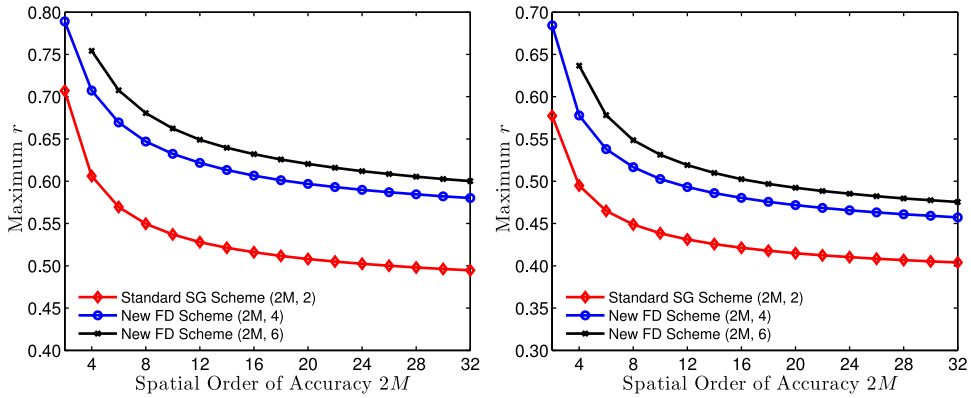

(a) Maximum allowed r for 2D modeling (b) Maximum allowed r for 3D modeling

Figure 3. The maximum allowed CFL number r for the standard staggered-grid finite-difference (FD) scheme ($2M$, 2), our new FD schemes ($2M$, 4) and ($2M$, 6) in (a) 2-D and (b) 3-D cases.

2.3 Comparison with the standard SGFD scheme

We compare our new FD schemes ($2M$, 4) and ($2M$, 6) with the standard SG scheme ($2M$, 2) using dispersion and stability analyses. Since the spatial order of accuracy is the same for all schemes, space dispersion errors should be similar if the same spatial grid spacing h is used. On one hand, we expect our new FD schemes are able to control time dispersion errors with a larger Δt than the standard SG scheme because the former has higher-order accuracy in time than the latter. On the other hand, the numerical stencils of our new FD schemes are larger than that of the standard SG scheme. This leaves the question of the overall computational efficiency of these schemes.

2.3.1 Stability analysis

We obtain the stability condition of the FD schemes using standard von Neumann analysis (e.g. Moczo *et al.* 2000; Liu & Sen 2009; Chen 2011). Fig. 3 displays the maximum allowed CFL number r for the standard SG scheme and our new FD schemes. Here r is defined as $r = c\Delta t/h$ for homogeneous wave speed c. With increasing order of accuracy in time, the stability condition becomes less stringent.

2.3.2 Dispersion analysis

We use a plane wave for dispersion analysis. A pressure plane wave p is given by

$$p(\boldsymbol{x}, t) = \exp[\mathrm{i}(\boldsymbol{k}\cdot\boldsymbol{x} - kc_{\mathrm{num}}t)], \tag{13}$$

where c_{num} is the numerical wave speed and the wavenumber $k = |\boldsymbol{k}|$. Substituting eq. (13) into eq. (3), we obtain the ratio of the numerical wave speed of our new FD scheme ($2M$, 4) to the true wave speed for 2-D modelling problems

$$\delta = \frac{c_{\mathrm{num}}}{c} = \frac{1}{rkh}\arccos(1 - 2g_2r^2),$$

where

$$g_2 = \left[\sum_{m=1}^{M} d_{m,0}\sin((m-1/2)k_xh) + 2d_{1,1}\sin(k_xh/2)\cos(k_zh)\right]^2 + \left[\sum_{m=1}^{M} d_{m,0}\sin((m-1/2)k_zh) + 2d_{1,1}\sin(k_zh/2)\cos(k_xh)\right]^2.$$

We assume the plane wave propagates in the direction of θ, that is, $\boldsymbol{k} = (k_x, k_z)^{\mathrm{T}} = k(\cos\theta, \sin\theta)^{\mathrm{T}}$. Then δ depends on angle θ. Because of symmetry, it is sufficient to investigate the cases with $\theta \in [0, \pi/4]$.

Fig. 4 shows the dispersion errors of the standard SGFD scheme ($2M$, 2) and our new FD schemes ($2M$, 4) and ($2M$, 6) when $2M = 16$ for 2-D modelling. Even for a small time interval with $r = 0.15$, the standard SGFD scheme ($2M$, 2) (Fig. 4a) is a little less accurate than our new FD scheme ($2M$, 4) (Fig. 4c). When increasing the time interval such that $r = 0.4$, the dispersion errors of our new FD schemes ($2M$, 4) and ($2M$, 6) (Figs 4d and e) are much smaller than those of the standard SGFD scheme ($2M$, 2) (Fig. 4b). Further increasing the time interval such that $r = 0.6$, the dispersion errors of our new FD scheme ($2M$, 6) (Fig. 4f) are still similar to those of our new FD scheme ($2M$, 4) with $r = 0.4$ (Fig. 4d). The dispersion errors in Fig. 4(a) and those in Figs 4(c)–(f) are similar to one another. Note that $r = 0.6$ is close to the maximum allowed value determined by stability condition for the scheme ($2M$, 6). We have similar observations for 3-D modelling, as demonstrated in Fig. 5.

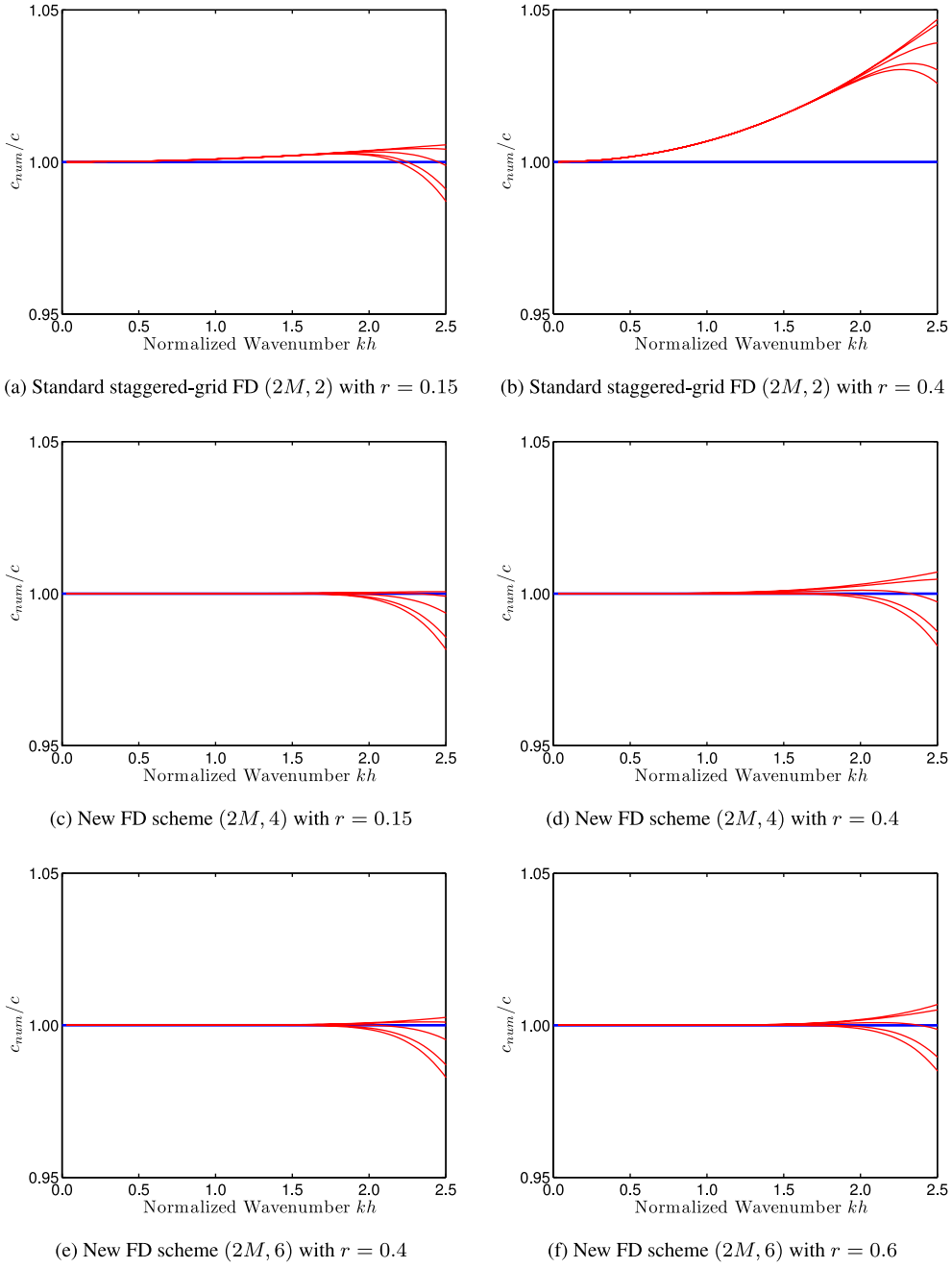

(a) Standard staggered-grid FD $(2M, 2)$ with $r = 0.15$

(b) Standard staggered-grid FD $(2M, 2)$ with $r = 0.4$

(c) New FD scheme $(2M, 4)$ with $r = 0.15$

(d) New FD scheme $(2M, 4)$ with $r = 0.4$

(e) New FD scheme $(2M, 6)$ with $r = 0.4$

(f) New FD scheme $(2M, 6)$ with $r = 0.6$

Figure 4. Dispersion relations for the standard staggered-grid (SG) FD scheme (2*M*, 2) (top row), our new FD scheme (2*M*, 4) (middle row) and our new FD scheme (2*M*, 6) (bottom row) for 2-D modelling. The spatial order of accuracy is $2M = 16$. The five red curves in each panel represent propagation angles $\theta = 0, \pi/16, \cdots, 4\pi/16$. The dispersion errors of the new scheme (2*M*, 4) with $r = 0.4$ in (d) are much smaller than those of the standard SGFD scheme with the same value of r in (b). The new scheme (2*M*, 6) further decreases the dispersion errors in (e). The dispersion curves in (a) and (c)–(f) are similar to one another.

2.3.3 Analysis of the computational efficiency for the new FD schemes

We compare the overall computational efficiency of the new FD schemes with the standard SGFD scheme for homogeneous media, and give the theoretical speed-up factors of our new schemes in Table 1 for 2-D modelling when $2M = 16$ (16th-order accuracy in space). The new schemes generally speed up the calculation by a factor of two to three compared to the standard SGFD scheme for a given 2-D modelling problem. Our new FD scheme (2*M*, 6) is the most efficient one among the three schemes.

We carry out the same analysis for 3-D modelling when $2M = 16$, as demonstrated in Table 2. Our new FD scheme (2*M*, 6) becomes less efficient than the scheme (2*M*, 4), since the former significantly increases the amount of floating-point operations at each time step compared to the standard SGFD scheme. Our new FD scheme (2*M*, 4) speeds up the calculation by a factor of approximately two compared to the standard SGFD scheme for a given 3-D modelling problem.

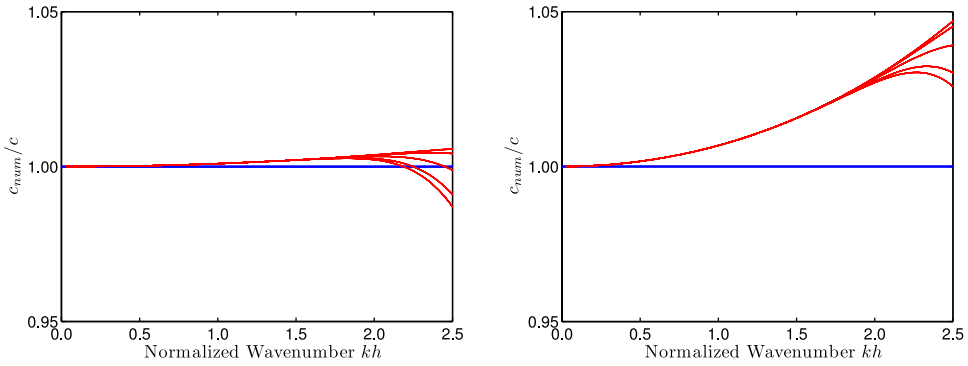

(a) Standard staggered-grid FD $(2M, 2)$ with $r = 0.15$ (b) Standard staggered-grid FD $(2M, 2)$ with $r = 0.4$

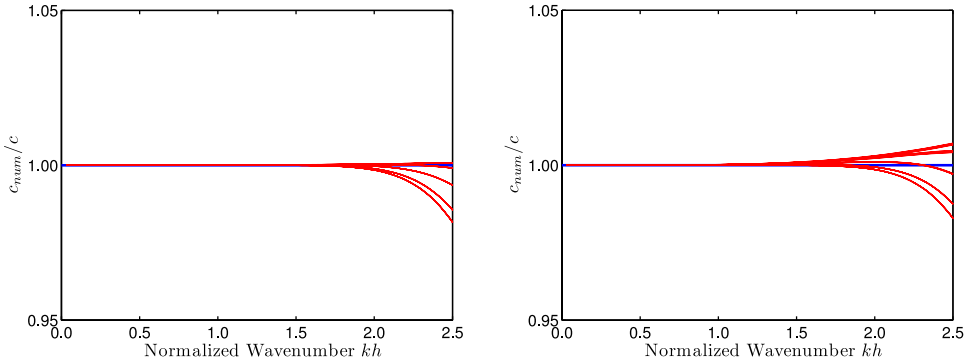

(c) New FD scheme $(2M, 4)$ with $r = 0.15$ (d) New FD scheme $(2M, 4)$ with $r = 0.4$

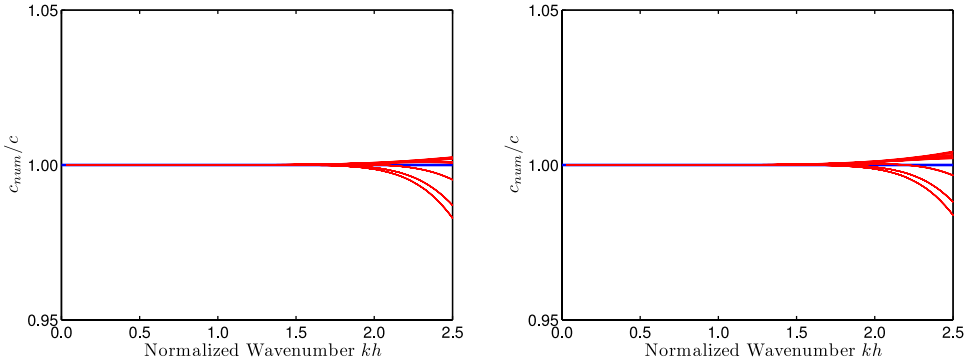

(e) New FD scheme $(2M, 6)$ with $r = 0.4$ (f) New FD scheme $(2M, 6)$ with $r = 0.5$

Figure 5. Dispersion relations for the standard staggered-grid (SG) FD scheme (2*M*, 2) (top row), our new FD scheme (2*M*, 4) (middle row) and our new FD scheme (2*M*, 6) (bottom row) for 3-D modelling. The spatial order of accuracy is $2M = 16$. The 25 red curves in each panel represent propagation angles $\theta = 0$, $\pi/16, \cdots, 4\pi/16$, $\phi = 0, \pi/16, \cdots, 4\pi/16$. Note that many of the 25 dispersion curves overlap with one another. The dispersion errors of the new scheme (2*M*, 4) with $r = 0.4$ in (d) are much smaller than those of the standard SG scheme with the same value of r in (b). The new scheme (2*M*, 6) further decreases the dispersion errors in (e). The dispersion curves in (a) and (c)–(f) are similar to one another. (a) Standard SGFD (2*M*, 2) with $r = 0.15$; (b) standard SGFD (2*M*, 2) with $r = 0.4$; (c) new FD scheme (2*M*, 4) with $r = 0.15$; (d) new FD scheme (2*M*, 4) with $r = 0.4$; (e) new FD scheme (2*M*, 6) with $r = 0.4$; (f) new FD scheme (2*M*, 6) with $r = 0.5$.

3 NUMERICAL EXAMPLES

We employ our new FD schemes to simulate scalar-wave propagation in 2- and 3-D models, and compare the waveforms with analytical solutions and those obtained with a fine time interval. In all examples, we keep the spatial grid spacing h and the spatial order of accuracy $2M$ the same for our new FD schemes and the standard SGFD scheme. We vary the time interval Δt to study the effect of time dispersion errors. For the ease of comparison, we specify Δt using the global CFL number $r_{\max}$ through $\Delta t = r_{\max} h/c_{\max}$, where $c_{\max}$ is the maximum wave speed of a model.

Table 1. The first two columns compare the standard staggered-grid (SG) scheme with our new FD schemes in the stencil size and the number of floating-point operations needed to compute one spatial derivative for 2-D modelling. To have similar dispersion errors when $2M = 16$, relative time intervals determined by dispersion analysis in Fig. 4 are listed in the third column. Combining the second and third columns, we obtain the theoretical speed-up factors of the new FD schemes compared with the standard SGFD scheme for 2-D modelling, as listed in the last column.

	Stencil size	Number of operations	Time interval	Theoretical speed-up
Standard SGFD ($2M$, 2)	$2M$	$3M$	Δt	1.0
New scheme ($2M$, 4)	$2M + 4$	$3M + 5$	$2.7\Delta t$	2.2
New scheme ($2M$, 6)	$2M + 12$	$3M + 14$	$4\Delta t$	2.5

Table 2. The first two columns compare the standard staggered-grid (SG) FD scheme with our new FD schemes in the stencil size and the number of floating-point operations needed to compute one spatial derivative for 3-D modelling. To have similar dispersion errors when $2M = 16$, relative time intervals determined by dispersion analysis in Fig. 5 are listed in the third column. Combining the second and third columns, we obtain the theoretical speed-up factors of the new FD schemes compared with the standard SGFD scheme for 3-D modelling, as listed in the last column.

	Stencil size	Number of operations	Time interval	Theoretical speed-up
Standard SGFD ($2M$, 2)	$2M$	$3M$	Δt	1.0
New scheme ($2M$, 4)	$2M + 8$	$3M + 9$	$2.7\Delta t$	1.9
New scheme ($2M$, 6)	$2M + 32$	$3M + 35$	$3.3\Delta t$	1.4

We use the coda-wave interferometry method to quantify the time-shift between synthetic waveforms $u_1(t)$ and $u_2(t)$ obtained using different approaches (Snieder *et al.* 2002). We compute the time-shifted cross-correlation over a time window with a width of t_w at the centre time t using

$$R(t_s) = \frac{\int_{t-t_w}^{t+t_w} u_1(t')u_2(t'+t_s)\,dt'}{\left[\int_{t-t_w}^{t+t_w} (u_1(t'))^2\,dt' \int_{t-t_w}^{t+t_w} (u_2(t'+t_s))^2\,dt'\right]^{1/2}}, \tag{14}$$

where t_s is the time-shift. When $u_2(t) = u_1(t-\tau)$ is a time-shifted version of $u_1(t)$, $R(t_s)$ attains its maximum at $t_s = \tau$. In the general case, we obtain t_{max} as the time-shift between two waveforms $u_1(t)$ and $u_2(t)$ when $R(t_s)$ attains its maximum at $t_s = t_{max}$. When the two waveforms are identical, the maximum value of the time-shifted cross-correlation is equal to unity at the zero lag time, that is $R(t_s = 0) = 1$.

3.1 2-D examples

3.1.1 Two-layer model with a low velocity contrast

Our first example is modelling of scalar-wave propagation in a 2-D layered velocity model defined by

$$c(x,z) = \begin{cases} c_1, & 0\text{ m} \le z \le 3000\text{ m}; \\ c_2, & 3000\text{ m} < z \le 4000\text{ m}. \end{cases} \tag{15}$$

We first set $c_1 = 3000\text{ m s}^{-1}$ and $c_2 = 3300\text{ m s}^{-1}$ such that the velocity contrast is low: $c_2/c_1 = 1.1$. The model is defined on a 2-D grid with $x \in [-2000\text{ m}, 2000\text{ m}]$ and $z \in [0\text{ m}, 4000\text{ m}]$. A Ricker-wavelet source with a central frequency of $f_0 = 40$ Hz is located at $(-1534\text{ m}, 80\text{ m})$. The receiver is located at (0 m, 1880 m) (a receiver for vertical seismic profiling survey). The spatial grid spacing of the model is $h = 8$m. We use our new FD schemes and the standard SGFD scheme, all with 16th-order accuracy in space, to generate synthetic waveforms at the receiver.

Fig. 6 shows the waveforms calculated using (I) the standard SGFD scheme with $r_{max} = 0.15$, (II) the standard SGFD scheme with $r_{max} = 0.33$, (III) the new FD scheme ($2M$, 4) with $r_{max} = 0.33$, (IV) the new FD scheme ($2M$, 4) with $r_{max} = 0.4$, (V) the new FD scheme ($2M$, 6) with $r_{max} = 0.4$, and (VI) the new FD scheme ($2M$, 6) with $r_{max} = 0.6$. We observe huge time dispersion errors in both the direct-arrival waveform and reflected waveform calculated using the standard SGFD scheme with $r_{max} = 0.33$ (Trace II in Figs 6a and b). To reduce the dispersion errors, we have to reduce the time interval to less than a half such that $r_{max} = 0.15$ for the standard SGFD scheme. Even so, the modelling error is still significant in the reflected waveform (Trace I in Fig. 6b). By contrast, our new FD scheme ($2M$, 4) is able to accurately model the waves with the large time interval with $r_{max} = 0.33$ (Trace III in Figs 6a and b). Using an even larger time interval with $r_{max} = 0.4$ in our new FD schemes ($2M$, 4) and ($2M$, 6) gives satisfactory modelling results (Traces IV and V in Figs 6a and b). Our new FD scheme ($2M$, 6) is able to handle the largest time interval with $r_{max} = 0.6$ among the three schemes (Trace VI in Figs 6a and b).

The time dispersion errors are quantified in Table 3 using coda-wave interferometry. We use the Cagniard–de Hoop method to generate reference waveforms for comparison with FD modelling results (e.g. Cagniard 1962). Table 3 shows that the relative time-shift errors t_{max}/T_0 are all 0.0 per cent for our new FD schemes, where T_0 is the central period of waveforms. These errors are 1.5 per cent for the direct-arrival

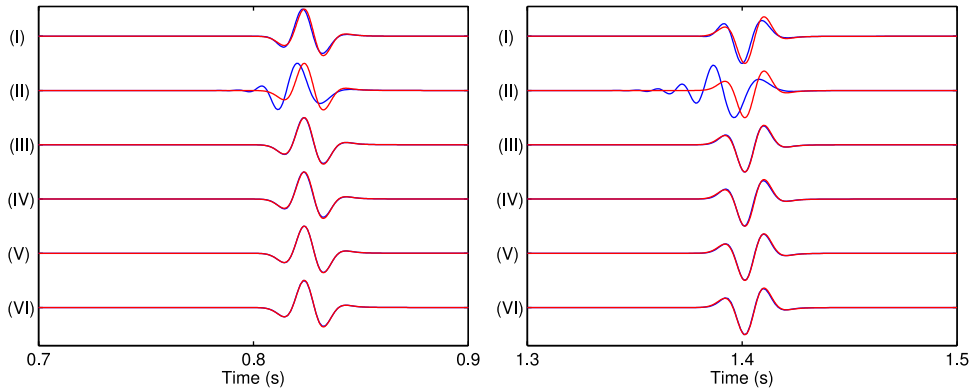

(a) Direct-arrival waveform (b) Reflected waveform

Figure 6. (a) Direct-arrival waveforms and (b) reflected waveforms calculated using (I) the standard staggered-grid (SG) FD scheme with $r_{max} = 0.15$, (II) the standard SGFD scheme with $r_{max} = 0.33$, (III) the new FD scheme ($2M$, 4) with $r_{max} = 0.33$, (IV) the new FD scheme ($2M$, 4) with $r_{max} = 0.4$, (V) the new FD scheme ($2M$, 6) with $r_{max} = 0.4$ and (VI) the new FD scheme ($2M$, 6) with $r_{max} = 0.6$ for the 2-D layered model (15) with velocity contrast $c_2/c_1 = 1.1$. The red line is the reference waveform obtained using the Cagniard–de Hoop method (e.g. Cagniard 1962); the blue line is the calculated waveform. Significant time dispersion errors exist in (I) and (II). The new FD schemes give accurate waveforms in (III)–(VI).

Table 3. Relative time-shift t_{max}/T_0 and maximum time-shifted cross-correlation $R(t_{max})$ between the calculated waveform and the reference waveform for the 2-D layered model with velocity contrast $c_2/c_1 = 1.1$. $T_0 = 1/f_0$ is the central wave period. The new FD schemes obviously give more accurate results than the standard staggered-grid (SG) FD scheme. The actual speed-up factors listed in the last column are calculated using the CPU times listed in the second-to-last column. To obtain the same modelling accuracy, our new FD scheme ($2M$, 6) is the most efficient among all the schemes.

	Direct-arrival waveform		Reflected waveform		CPU time (s)	Speed-up
	t_{max}/T_0	$R(t_{max})$	t_{max}/T_0	$R(t_{max})$		
Standard SGFD ($r_{max} = 0.15$)	1.5 per cent	0.995	4.4 per cent	0.988	224	1.0
Standard SGFD ($r_{max} = 0.33$)	9.6 per cent	0.930	58 per cent	0.904	102	–
New FD scheme ($2M$, 4) ($r_{max} = 0.33$)	0.0 per cent	0.999	0.0 per cent	0.998	140	1.6
New FD scheme ($2M$, 4) ($r_{max} = 0.4$)	0.0 per cent	0.999	0.0 per cent	0.997	116	1.9
New FD scheme ($2M$, 6) ($r_{max} = 0.4$)	0.0 per cent	1.000	0.0 per cent	0.999	133	1.7
New FD scheme ($2M$, 6) ($r_{max} = 0.6$)	0.0 per cent	1.000	0.0 per cent	0.998	89	2.5

waveform and 4.4 per cent for the reflected waveform for the standard SGFD scheme with $r_{max} = 0.15$, and these errors increase up to almost 60 per cent when $r_{max} = 0.33$. The maximum values of the time-shifted cross-correlations between simulated waveforms and the reference waveforms are at least 0.997 for our new FD schemes (rows 3–6 in Table 3), and those for the standard SGFD modelings range from 0.930 to 0.995 for the direct-arrival waveforms and 0.904 to 0.988 for the reflected waveforms. CPU times used by different schemes and speed-up factors are listed in the last two columns of Table 3. The speed-up factors of our new FD schemes relative to the standard SGFD scheme with $r_{max} = 0.15$ range from 1.6 to 2.5, and our new FD schemes generate more accurate synthetic waveforms than the standard SGFD scheme. Among our new FD schemes, the scheme ($2M$, 6) speeds up the most for this 2-D modelling example. The actual speed-up factor of our new FD scheme ($2M$, 4) is 1.9, which is a little lower than the theoretical estimate of 2.2 as listed in Table 1.

3.1.2 Two-layer model with a large velocity contrast

We next perform numerical modelings for this 2-D model with a large velocity contrast of 5, and compare the accuracy and computational efficiency of different FD schemes. We set $c_1 = 1500\ \mathrm{m\,s^{-1}}$ and $c_2 = 7500\ \mathrm{m\,s^{-1}}$ such that the velocity contrast $c_2/c_1 = 5$. The central frequency of the Ricker wavelet is $f_0 = 20$ Hz, while all the other parameters are the same as the previous example. The dispersion errors and computational times of the standard SGFD schemes and our new FD schemes ($2M$, 4) and ($2M$, 6) are tabulated in Table 4. The values of relative time-shift errors t_{max}/T_0 are similar for all FD schemes. The standard SGFD scheme gives much smaller errors compared with the low velocity contrast case, as shown in Table 3. This is mainly because the modelling for the large velocity contrast has to use a much smaller time interval than that used in the numerical modelling for the model with a low velocity contrast. Our new FD schemes ($2M$, 4) and ($2M$, 6) are approximately twice faster than the standard SGFD scheme. Our FD scheme ($2M$, 6) is a little less efficient than our FD scheme ($2M$, 4) for this large velocity contrast example because the maximum time interval is limited by the stability condition.

Our numerical experiments demonstrate that our new FD schemes lose their advantages over the standard SGFD scheme if the velocity contrast increases to 10. However, for most large-scale geophysical applications, the velocity contrasts often range approximately from 1 to 3.

Table 4. Relative time-shift t_{max}/T_0 and maximum time-shifted cross-correlation $R(t_{max})$ between the calculated waveform and the reference waveform for the 2-D layered model with velocity contrast $c_2/c_1 = 5$. $T_0 = 1/f_0$ is the central wave period. The actual speed-up factors listed in the last column are calculated using the CPU times listed in the second-to-last column. The standard staggered-grid (SG) FD scheme gives much smaller errors compared with the low velocity contrast case, as shown in Table 3. To obtain the same modelling accuracy, our new FD scheme (2*M*, 4) is the most efficient among all the schemes.

	Direct-arrival waveform		Reflected waveform		CPU time (s)	Speed-up
	t_{max}/T_0	$R(t_{max})$	t_{max}/T_0	$R(t_{max})$		
Standard SGFD ($r_{max} = 0.2$)	0.2 per cent	1.000	0.6 per cent	1.000	805	1.0
New FD scheme (2*M*, 4) ($r_{max} = 0.5$)	0.0 per cent	1.000	0.2 per cent	1.000	434	1.9
New FD scheme (2*M*, 4) ($r_{max} = 0.6$)	0.0 per cent	1.000	0.6 per cent	1.000	361	2.2
New FD scheme (2*M*, 6) ($r_{max} = 0.63$)	0.0 per cent	1.000	0.4 per cent	1.000	392	2.0

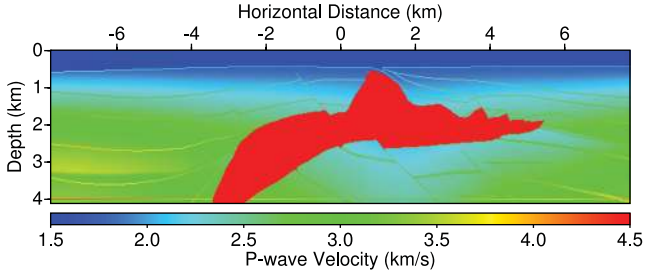

Figure 7. The 2-D Society of Exploration Geophysicists/European Association of Geoscientists and Engineers (SEG/EAGE) salt model for scalar-wave modelling.

3.1.3 2-D SEG/EAGE salt model

Next, we study the accuracy and efficiency of our new FD schemes for modelling scalar-wave propagation in 2-D complex media. We compare synthetic waveforms obtained using our new FD scheme (2*M*, 4) with those produced with the standard SGFD scheme for the 2-D Society of Exploration Geophysicists/European Association of Geoscientists and Engineers (SEG/EAGE) salt model depicted in Fig. 7. Both FD schemes have 16th-order accuracy in space. A Ricker-wavelet source with a central frequency of 8 Hz is located at (0 m, 125 m), and the receiver array is located at the same depth. The model grid spacing is $h = 25$ m. We use the standard SGFD scheme with a tiny time interval with $r_{max} = 0.025$ to generate reference waveforms, and the resulting common-shot gather is shown in Fig. 8.

Fig. 9 shows the waveforms calculated using (I) the standard SGFD scheme with $r_{max} = 0.2$, (II) the standard SGFD scheme with $r_{max} = 0.5$, (III) the new FD scheme (2*M*, 4) with $r_{max} = 0.5$ and (IV) the new FD scheme (2*M*, 4) with $r_{max} = 0.6$ at Receivers #1 and #2 with offsets −2000 m and 2000 m, respectively. The time dispersion errors are quantified in Figs 10 and 11. The standard SGFD scheme with $r_{max} = 0.5$ gives significant mismatch between the calculated waveforms and the reference waveforms. The errors are mostly reduced if we decrease the time interval such that $r_{max} = 0.2$ for the standard SGFD scheme. Our new FD scheme (2*M*, 4) with $r_{max} = 0.6$ introduces few time-shift errors at both receivers. According to the CPU times listed in Table 5, our new FD scheme (2*M*, 4) is 2.1 times more efficient than the standard SGFD scheme. For this salt model with the largest velocity contrast of 2.94, our new FD scheme (2*M*, 6) is not able to further improve the efficiency, since its time interval is restricted by the stability condition.

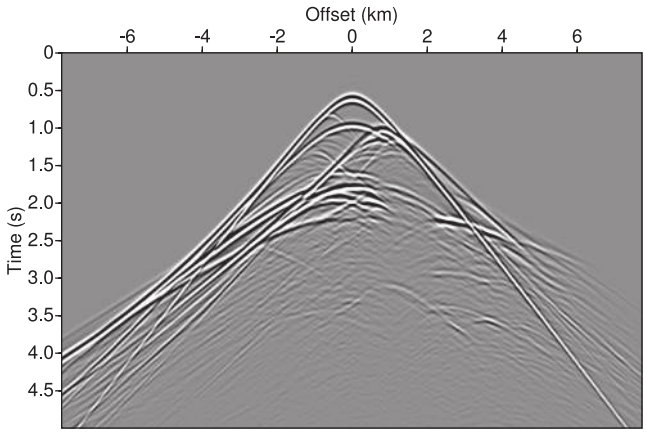

Figure 8. The common-shot gather calculated using the standard staggered-grid FD scheme with a tiny time interval with $r_{max} = 0.025$ for the 2-D SEG/EAGE salt model.

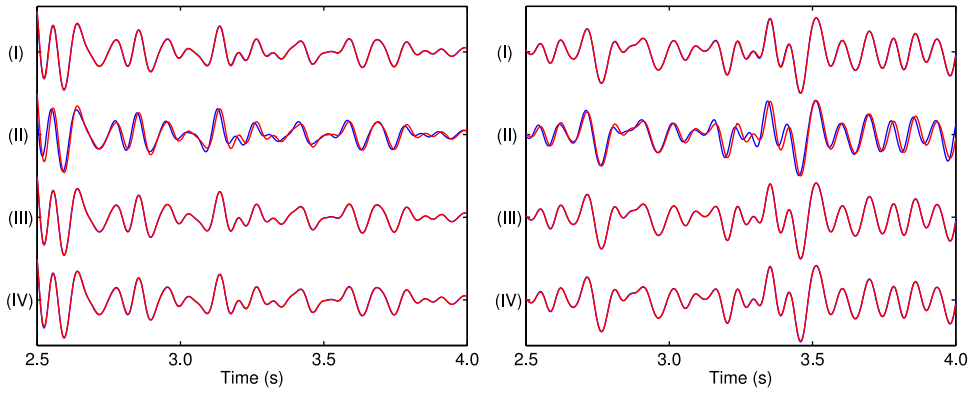

(a) Receiver #1 (b) Receiver #2

Figure 9. Waveforms at (a) Receiver #1 and (b) Receiver #2 calculated using (I) the standard staggered-grid (SG) FD scheme with $r_{\max} = 0.2$, (II) the standard SGFD scheme with $r_{\max} = 0.5$, (III) the new FD scheme ($2M$, 4) with $r_{\max} = 0.5$, and (IV) the new FD scheme ($2M$, 4) with $r_{\max} = 0.6$ for the 2-D SEG/EAGE salt model. The red line is the reference waveform calculated using the standard SGFD scheme with a tiny time interval with $r_{\max} = 0.025$; the blue line is the calculated waveform. The waveforms in (II) mismatch the reference waveforms. We have to use a small time interval for the standard SGFD scheme to reduce the errors, as shown in (I). Our new FD scheme ($2M$, 4) is able to handle large time intervals and gives well-matched waveforms in (III) and (IV).

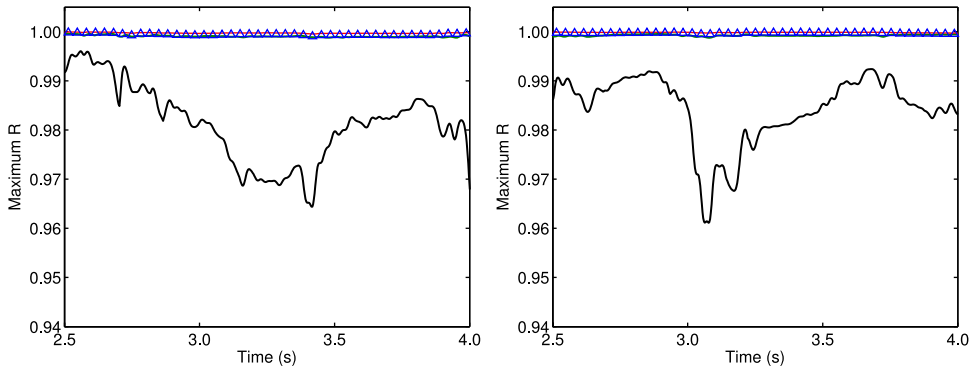

(a) Receiver #1 (b) Receiver #2

Figure 10. Maximum time-shifted cross-correlation $R(t_{\max})$ between the calculated waveform and the reference waveform at (a) Receiver #1 and (b) Receiver #2 for the 2-D SEG/EAGE salt model. Dark green line: the standard staggered-grid (SG) FD scheme with $r_{\max} = 0.2$; black line: the standard SGFD scheme with $r_{\max} = 0.5$; red line: the new FD scheme ($2M$, 4) with $r_{\max} = 0.5$; blue symbols: the new FD scheme ($2M$, 4) with $r_{\max} = 0.6$. The width of the time window is $t_w = 2T_0$ in eq. (14), where T_0 is the central wave period. The new FD scheme ($2M$, 4) gives more accurate waveforms than the standard SGFD scheme.

3.2 3-D examples

We conduct modelling of scalar-wave propagation in a 3-D layered model and the 3-D SEG/EAGE salt model using our new FD schemes and the standard SGFD scheme, and compare the accuracy and efficiency of the schemes.

3.2.1 Two-layer model

The velocity of the layered model is defined by

$$c(x, y, z) = \begin{cases} c_1 = 3000 \text{ m s}^{-1}, & 0 \text{ m} \le z \le 2000 \text{ m}; \\ c_2 = 3300 \text{ m s}^{-1}, & 2000 \text{ m} < z \le 3000 \text{ m}. \end{cases} \tag{16}$$

A Ricker-wavelet source with a central frequency of 40 Hz is located at (−1000 m, 1000 m, 180 m). The receiver is located at (0 m, 0 m, 1080 m). The model grid spacing for the 3-D layered model is $h = 8$ m. The FD schemes used have 16th-order accuracy in space to control the spatial dispersion error. Fig. 12 displays the waveforms calculated using (I) the standard SGFD scheme with $r_{\max} = 0.15$, (II) the standard SGFD scheme with $r_{\max} = 0.29$, (III) the new FD scheme ($2M$, 4) with $r_{\max} = 0.29$, (IV) the new FD scheme ($2M$, 4) with $r_{\max} = 0.4$, (V) the new FD scheme ($2M$, 6) with $r_{\max} = 0.4$ and (VI) the new FD scheme ($2M$, 6) with $r_{\max} = 0.5$. The time dispersion errors are quantified in Table 6. From this table, we observe that the standard SGFD scheme with $r_{\max} = 0.29$ gives large dispersion errors. Reducing the time interval such that $r_{\max} = 0.15$ suppresses the dispersion errors, but they are still quite significant. Our new FD scheme ($2M$, 4) with $r_{\max} = 0.29$ or $r_{\max} = 0.4$ generates waveforms with very small dispersion errors. The new FD scheme ($2M$, 6) is able to handle a large time

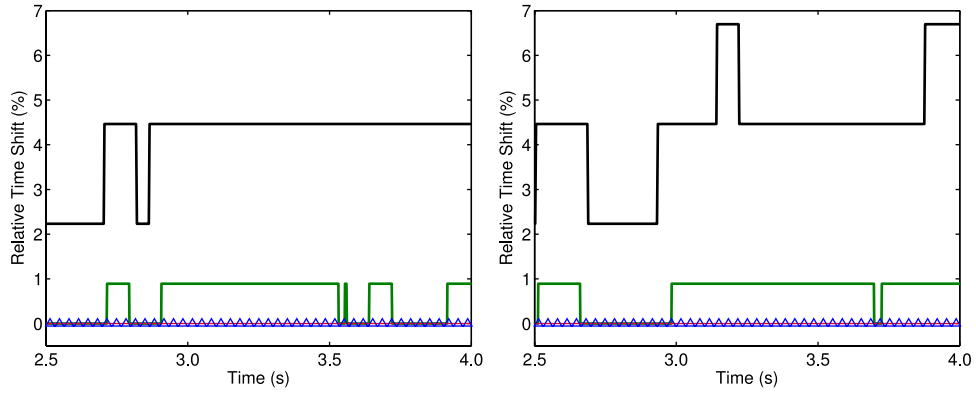

(a) Receiver #1 (b) Receiver #2

Figure 11. Relative time-shift $t_{\max}/T_0$ between the calculated waveform and the reference waveform at (a) Receiver #1 and (b) Receiver #2 for the 2-D SEG/EAGE salt model. Dark green line: the standard staggered-grid (SG) FD scheme with $r_{\max} = 0.2$; black line: the standard SGFD scheme with $r_{\max} = 0.5$; red line: the new FD scheme ($2M$, 4) with $r_{\max} = 0.5$; blue symbols: the new FD scheme ($2M$, 4) with $r_{\max} = 0.6$. The standard SGFD scheme with $r_{\max} = 0.5$ leads to significant time-shift errors in the calculated waveforms, while our new FD scheme ($2M$, 4) introduces few time-shift errors at both receivers.

Table 5. Comparison of the CPU times needed by the standard staggered-grid (SG) FD scheme with $r_{\max} = 0.2$ and our new FD scheme ($2M$, 4) with $r_{\max} = 0.6$ for the 2-D SEG/EAGE salt model. Both schemes lead to similar modelling accuracy, while our new FD scheme ($2M$, 4) is 2.1 times faster.

	Standard SGFD with $r_{\max} = 0.2$	New scheme ($2M$, 4) with $r_{\max} = 0.6$
CPU time (s)	119	55.6
Speed-up factor	1.0	2.1

interval such that $r_{\max} = 0.5$. Our new FD scheme ($2M$, 4) is the most efficient among all the schemes according to the CPU times listed in Table 6. It speeds up the calculation by a factor of 1.8 relative to the standard SGFD scheme.

As demonstrated for the 2-D layered model, our numerical tests show that our new FD scheme ($2M$, 6) becomes even less efficient than the FD scheme ($2M$, 4) for the 3-D layered model with a large velocity contrast.

3.2.2 3-D SEG/EAGE salt model

Our last modelling example is simulation of scalar-wave propagation in the 3-D SEG/EAGE salt model in Fig. 13. A Ricker-wavelet source with a central frequency of 12 Hz is located at (0 m, 0 m, 100 m). The model grid spacing is $h = 20$ m. The FD schemes used have 32nd-order accuracy in space. Fig. 14 shows the reference common-shot gather calculated using the standard SGFD scheme with a tiny time interval with $r_{\max} = 0.025$. This common-shot gather contains more complicated waveforms than those in 2-D case as shown in Fig. 8 because of

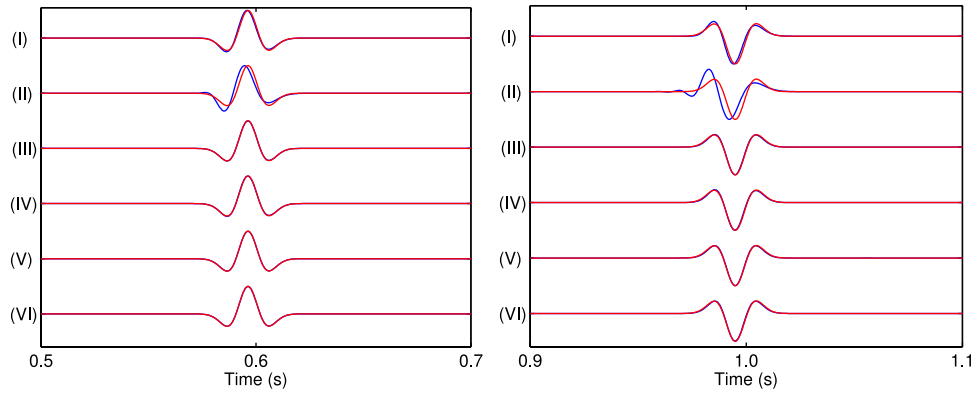

(a) Direct-arrival waveform (b) Reflected waveform

Figure 12. (a) Direct-arrival waveforms and (b) reflected waveforms calculated using (I) the standard staggered-grid (SG) FD scheme with $r_{\max} = 0.15$, (II) the standard SGFD scheme with $r_{\max} = 0.29$, (III) the new FD scheme ($2M$, 4) with $r_{\max} = 0.29$, (IV) the new FD scheme ($2M$, 4) with $r_{\max} = 0.4$, (V) the new FD scheme ($2M$, 6) with $r_{\max} = 0.4$ and (VI) the new FD scheme ($2M$, 6) with $r_{\max} = 0.5$. The red line is the reference waveform; the blue line is the calculated waveform. Significant time dispersion errors exist if we use the standard SGFD scheme. The new FD schemes give accurate waveforms in (III–VI).

Table 6. Relative time-shift t_{max}/T_0 and maximum time-shifted cross-correlation $R(t_{max})$ between the calculated waveform and the reference waveform for the 3-D layered model with velocity contrast $c_2/c_1 = 1.1$. $T_0 = 1/f_0$ is the central wave period. The new FD schemes obviously give more accurate results than the standard staggered-grid (SG) FD scheme. The actual speed-up factors listed in the last column are calculated using the CPU times listed in the second-to-last column. To obtain the same modelling accuracy, our new FD scheme ($2M$, 4) is the most efficient among all the schemes.

	Direct-arrival waveform		Reflected waveform		CPU time (s)	Speed-up
	t_{max}/T_0	$R(t_{max})$	t_{max}/T_0	$R(t_{max})$		
Standard SGFD ($r_{max} = 0.15$)	1.5 per cent	0.999	2.9 per cent	0.994	2.35E5	1.0
Standard SGFD ($r_{max} = 0.29$)	5.6 per cent	0.982	8.4 per cent	0.949	1.21E5	–
New FD scheme ($2M$, 4) ($r_{max} = 0.29$)	0.0 per cent	1.000	0.0 per cent	0.999	1.81E5	1.3
New FD scheme ($2M$, 4) ($r_{max} = 0.4$)	0.0 per cent	1.000	0.0 per cent	0.998	1.31E5	1.8
New FD scheme ($2M$, 6) ($r_{max} = 0.4$)	0.0 per cent	1.000	0.0 per cent	0.999	1.67E5	1.4
New FD scheme ($2M$, 6) ($r_{max} = 0.5$)	0.0 per cent	1.000	0.0 per cent	0.998	1.34E5	1.8

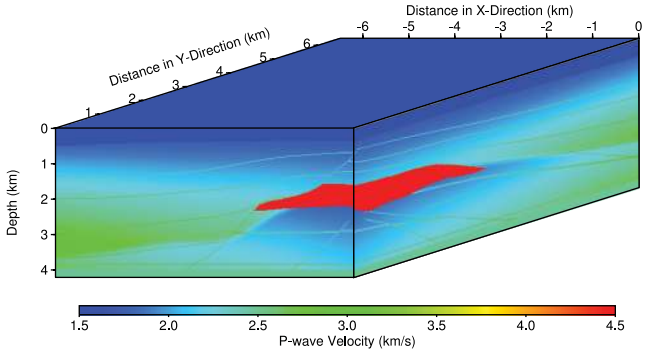

Figure 13. The 3-D SEG/EAGE salt model for scalar-wave modelling.

the 3-D propagation/reflection effects. Fig. 15 shows a comparison among waveforms calculated using (I) the standard SGFD scheme with $r_{max} = 0.15$, (II) the standard SGFD scheme with $r_{max} = 0.38$, (III) the new FD scheme ($2M$, 4) with $r_{max} = 0.38$ and (IV) the new FD scheme ($2M$, 4) with $r_{max} = 0.45$ at Receivers #1 and #2 with offsets of -2000 m and 2000 m along the x-direction, respectively. The time dispersion errors are quantified in Figs 16 and 17. Significant errors are observed for the standard SGFD scheme with $r_{max} = 0.38$. Both results of the standard SGFD scheme with $r_{max} = 0.15$ and our new FD scheme ($2M$, 4) with $r_{max} = 0.45$ well match the reference waveforms. Our new FD scheme ($2M$, 4) is again superior to the standard SGFD scheme because our new FD scheme speeds up the calculation by a factor of 2.2 relative to the latter, as shown in Table 7.

4 CONCLUSIONS

We have developed novel FD methods for solving 2- and 3-D scalar-wave equations on SGs. Our new FD schemes, denoted by ($2M$, 4) or ($2M$, 6), are $2M$-th-order accurate in space and fourth- or sixth-order accurate in time. The requirement of our new methods for computer

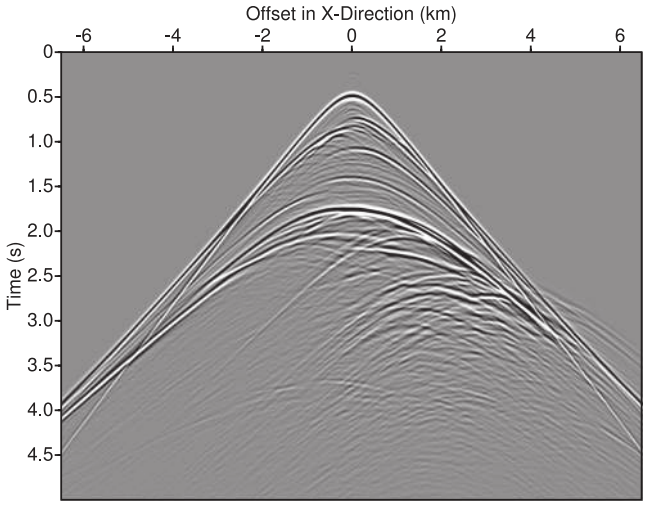

Figure 14. The common-shot gather calculated using the standard staggered-grid FD scheme with a tiny time interval with $r_{max} = 0.025$ for the 3-D SEG/EAGE salt model. The receiver array is along x-axis.

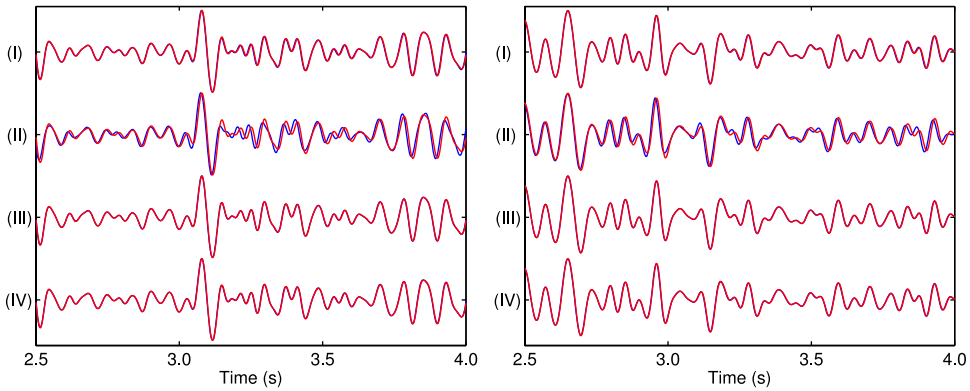

(a) Receiver #1 (b) Receiver #2

Figure 15. Waveforms at (a) Receiver #1 and (b) Receiver #2 calculated using (I) the standard staggered-grid (SG) FD scheme with $r_{\max} = 0.15$, (II) the standard SGFD scheme with $r_{\max} = 0.38$, (III) the new FD scheme ($2M$, 4) with $r_{\max} = 0.38$ and (IV) the new FD scheme ($2M$, 4) with $r_{\max} = 0.45$ for the 3-D SEG/EAGE salt model. The red line is the reference waveform calculated using the standard SGFD scheme with a tiny time interval with $r_{\max} = 0.025$; the blue line is the calculated waveform. The waveforms in (II) mismatch the reference waveforms. We have to use a small time interval for the standard SGFD scheme to reduce the errors, as shown in (I). Our new FD scheme ($2M$, 4) is able to handle large time intervals and gives well-matched waveforms in (III) and (IV).

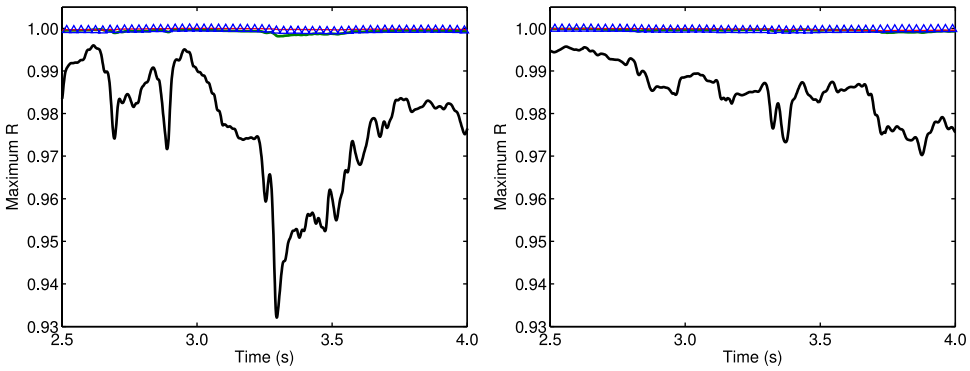

(a) Receiver #1 (b) Receiver #2

Figure 16. Maximum time-shifted cross-correlation $R(t_{\max})$ between the calculated waveform and the reference waveform at (a) Receiver #1 and (b) Receiver #2 for the 3-D SEG/EAGE salt model. Dark green line: the standard staggered-grid (SG) FD scheme with $r_{\max} = 0.15$; black line: the standard SGFD scheme with $r_{\max} = 0.38$; red line: the new FD scheme ($2M$, 4) with $r_{\max} = 0.38$; blue symbols: the new FD scheme ($2M$, 4) with $r_{\max} = 0.45$. The width of the time window is $t_w = 2T_0$ in eq. (14), where T_0 is the central wave period. The new FD scheme ($2M$, 4) gives more accurate waveforms than the standard SGFD scheme.

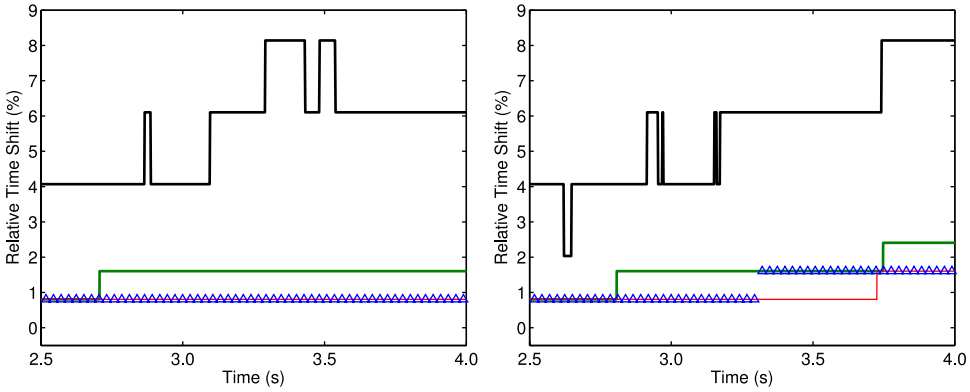

(a) Receiver #1 (b) Receiver #2

Figure 17. Relative time-shift $t_{\max}/T_0$ between the calculated waveform and the reference waveform at (a) Receiver #1 and (b) Receiver #2 for the 3-D SEG/EAGE salt model. Dark green line: the standard staggered-grid (SG) FD scheme with $r_{\max} = 0.15$; black line: the standard SGFD scheme with $r_{\max} = 0.38$; red line: the new FD scheme ($2M$, 4) with $r_{\max} = 0.38$; blue symbols: the new FD scheme ($2M$, 4) with $r_{\max} = 0.45$. The standard SGFD scheme with $r_{\max} = 0.38$ leads to significant time-shift errors in the calculated waveform, while our new FD scheme ($2M$, 4) introduces very small time-shift errors at both receivers.

Table 7. Comparison of the CPU times needed by the standard staggered-grid (SG) FD scheme with $r_{max} = 0.15$ and our new FD scheme (2M, 4) with $r_{max} = 0.45$. Both schemes lead to similar modelling accuracy, while our new FD scheme (2M, 4) is 2.2 times more efficient.

	Standard SGFD with $r_{max} = 0.15$	New scheme (2M, 4) with $r_{max} = 0.45$
CPU time (s)	6.43E5	2.91E5
Speed-up factor	1.0	2.2

memory is almost the same as the standard SGFD scheme with second-order accuracy in time. We have validated the improved accuracy and computational efficiency of our new FD schemes using dispersion analysis and numerical modelling of scalar-wave propagation in 2- and 3-D complex models involving a wide range of velocity contrasts. Our scheme (2M, 4) is generally more efficient than our scheme (2M, 6) for complex media. For media with a velocity contrast up to five, our scheme (2M, 4) is approximately two times faster than the standard SGFD scheme to achieve the same modelling accuracy. Further numerical experiments demonstrate that our scheme (2M, 4) loses its advantages over the standard SGFD scheme if the velocity contrast is 10. However, for most large scale geophysical applications, the velocity contrasts often range approximately from 1 to 3. Our new FD scheme can significantly reduce the computational costs for large-scale 3-D reverse-time migration and full-waveform inversion. The strategy of our new FD scheme for scalar-wave propagation can be employed to improve the computational efficiency of FD modelling of elastic-wave propagation.

ACKNOWLEDGEMENTS

This work was supported by U.S. Department of Energy through contract DE-AC52-06NA25396 to Los Alamos National Laboratory (LANL). The computation was performed using supercomputers of LANL's Institutional Computing Program. We thank Editor Dr Andrea Morelli, Reviewer Dr Peter Moczo and an anonymous reviewer for providing us with their valuable comments to improve the quality of the paper.

REFERENCES

Blanch, J.O. & Robertsson, J.O.A., 1997. A modified Lax-Wendroff correction for wave propagation in media described by Zener elements, *Geophys. J. Int.,* **131**(2), 381–386.

Cagniard, L., 1962. *Reflection and Refraction of Progressive Seismic Waves, International Series in the Earth Sciences,* McGraw-Hill.

Chen, J.-B., 2011. A stability formula for Lax-Wendroff methods with fourth-order in time and general-order in space for the scalar wave equation, *Geophysics,* **76**(2), T37–T42.

Chu, C. & Stoffa, P., 2012. Determination of finite-difference weights using scaled binomial windows, *Geophysics,* **77**(3), W17–W26.

Dablain, M., 1986. The application of high-order differencing to the scalar wave equation, *Geophysics,* **51**(1), 54–66.

Etgen, J., Gray, S. & Zhang, Y., 2009. An overview of depth imaging in exploration geophysics, *Geophysics,* **74**(6), WCA5–WCA17.

Fornberg, B., 1998. Classroom note: calculation of weights in finite difference formulas, *SIAM Rev.,* **40**(3), 685–691.

Geller, R.J. & Takeuchi, N., 1995. A new method for computing highly accurate DSM synthetic seismograms, *Geophys. J. Int.,* **123**(2), 449–470.

Geller, R.J. & Takeuchi, N., 1998. Optimally accurate second-order time-domain finite difference scheme for the elastic equation of motion: one-dimensional case, *Geophys. J. Int.,* **135**(1), 48–62.

Holberg, O., 1987. Computational aspects of the choice of operator and sampling interval for numerical differentiation in large-scale simulation of wave phenomena, *Geophys. Prospect.,* **35**(6), 629–655.

Lax, P.D. & Wendroff, B., 1964. Difference schemes for hyperbolic equations with high order of accuracy, *Commun. Pure appl. Math.,* **17**(3), 381–398.

Levander, A.R., 1988. Fourth-order finite-difference P-SV seismograms, *Geophysics,* **53**(11), 1425–1436.

Liu, Y. & Sen, M.K., 2009. A new time-space domain high-order finite-difference method for the acoustic wave equation, *J. Comput. Phys.,* **228**(23), 8779–8806.

Liu, Y. & Sen, M.K., 2011. Scalar wave equation modeling with time-space domain dispersion-relation-based staggered-grid finite-difference schemes, *Bull. seism. Soc. Am.,* **101**(1), 141–159.

Liu, Y. & Sen, M.K., 2013. Time-space domain dispersion-relation-based finite-difference method with arbitrary even-order accuracy for the 2D acoustic wave equation, *J. Comput. Phys.,* **232**(1), 327–345.

Mizutani, H., Geller, R.J. & Takeuchi, N., 2000. Comparison of accuracy and efficiency of time-domain schemes for calculating synthetic seismograms, *Phys. Earth planet. Inter.,* **119**(1–2), 75–97.

Moczo, P., Kristek, J. & Halada, L., 2000. 3D fourth-order staggered-grid finite-difference schemes: stability and grid dispersion, *Bull. seism. Soc. Am.,* **90**(3), 587–603.

Moczo, P., Kristek, J., Vavryčuk, V., Archuleta, R.J. & Halada, L., 2002. 3D heterogeneous staggered-grid finite-difference modeling of seismic motion with volume harmonic and arithmetic averaging of elastic moduli and densities, *Bull. seism. Soc. Am.,* **92**(8), 3042–3066.

Moczo, P., Robertsson, J.O. & Eisner, L., 2007. The finite-difference time-domain method for modeling of seismic wave propagation, in *Advances in Wave Propagation in Heterogenous Earth, Advances in Geophysics,* Vol. 48, pp. 421–516, eds Ru-Shan Wu, V.M. & Dmowska, R., Elsevier.

Saenger, E.H., Gold, N. & Shapiro, S.A., 2000. Modeling the propagation of elastic waves using a modified finite-difference grid, *Wave Motion,* **31**(1), 77–92.

Snieder, R., Grłt, A., Douma, H. & Scales, J., 2002. Coda wave interferometry for estimating nonlinear behavior in seismic velocity, *Science,* **295**(5563), 2253–2255.

Song, X., Fomel, S. & Ying, L., 2013. Lowrank finite-differences and lowrank Fourier finite-differences for seismic wave extrapolation in the acoustic approximation, *Geophys. J. Int.,* **193**(2), 960–969.

Takeuchi, N. & Geller, R.J., 2000. Optimally accurate second order time-domain finite difference scheme for computing synthetic seismograms in 2-D and 3-D media, *Phys. Earth planet. Inter.,* **119**(1–2), 99–131.

Tam, C.K. & Webb, J.C., 1993. Dispersion-relation-preserving finite difference schemes for computational acoustics, *J. Comput. Phys.,* **107**(2), 262–281.

Virieux, J., 1984. SH-wave propagation in heterogeneous media: velocity-stress finite-difference method, *Geophysics,* **49**(11), 1933–1942.

Virieux, J., 1986. P-SV wave propagation in heterogeneous media: velocity-stress finite-difference method, *Geophysics,* **51**(4), 889–901.

Virieux, J. & Operto, S., 2009. An overview of full-waveform inversion in exploration geophysics, *Geophysics,* **74**(6), WCC1–WCC26.

Yee, K., 1966. Numerical solution of initial boundary value problems involving Maxwell's equations in isotropic media, *IEEE Trans. Antennas Propag.,* **14**(3), 302–307.

Zingg, D., 2000. Comparison of high-accuracy finite-difference methods for linear wave propagation, *SIAM J. Sci. Comput.,* **22**(2), 476–502.

APPENDIX: RELATIONSHIP BETWEEN OUR NEW FD SCHEME (2*M*, 4) AND A LAX-WENDROFF SCHEME

We show in the following that our new FD scheme (2*M*, 4) is similar to a Lax-Wendroff scheme where the high-order derivatives are approximated using a special discretization method. Without loss of generality, we consider 2-D modelling and assume the spatial order of accuracy $2M = 6$.

The Taylor expansion of the velocity wavefield with respect to time gives

$$u_{0,0}^{j+1/2} = u_{0,0}^{j-1/2} + \Delta t\,(u_t)_{0,0}^{j} + \frac{\Delta t^3}{24}\,(u_{ttt})_{0,0}^{j} + \frac{\Delta t^5}{1920}\,(u_{ttttt})_{0,0}^{j}\,, \tag{A1}$$

where $(0, 0)$ is the spatial grid point at (x, z). Assuming homogeneous media and replacing the time derivatives in eq. (A1) by spatial derivatives using eq. (1), we obtain a Lax-Wendroff scheme

$$u_{0,0}^{j+1/2} = u_{0,0}^{j-1/2} - \frac{\Delta t}{\rho h}\left[h p_x + \frac{r^2\,h^3}{24}\,(p_{xxx} + p_{xzz}) + \frac{r^4\,h^5}{1920}\,p_{xxxxx}\right], \tag{A2}$$

where we discard all mixed fifth derivatives and terms $p_{\dots}$ are given in the following. We approximate the derivatives along x-axis using a six-point stencil

$$\begin{aligned} h p_x &= \frac{75}{64}(p_{1/2,0} - p_{-1/2,0}) - \frac{25}{384}(p_{3/2,0} - p_{-3/2,0}) + \frac{3}{640}(p_{5/2,0} - p_{-5/2,0}),\\ h^3 p_{xxx} &= -\frac{17}{4}(p_{1/2,0} - p_{-1/2,0}) + \frac{13}{8}(p_{3/2,0} - p_{-3/2,0}) - \frac{1}{8}(p_{5/2,0} - p_{-5/2,0}),\\ h^5 p_{xxxxx} &= 10(p_{1/2,0} - p_{-1/2,0}) - 5(p_{3/2,0} - p_{-3/2,0}) + (p_{5/2,0} - p_{-5/2,0}). \end{aligned} \tag{A3}$$

The mixed derivative p_{xzz} is approximated using a six-point stencil containing two points on the axis and four points off the axis. Namely,

$$h^3 p_{xzz} = p_{1/2,1} - p_{-1/2,1} - 2p_{1/2,0} + 2p_{-1/2,0} + p_{1/2,-1} - p_{-1/2,-1}. \tag{A4}$$

Substituting eqs (A3) and (A4) into eq. (A2), we obtain our new FD scheme (2*M*, 4):

$$u_{0,0}^{j+1/2} = u_{0,0}^{j-1/2} - \frac{\Delta t}{\rho} D_x^{2M,4} p_{0,0}^{j}, \tag{A5}$$

where the FD operator $D_x^{2M,4}$ is defined in eq. (4). Note that the standard Lax-Wendroff FD schemes (Dablain 1986; Chen 2011) do not contain term $\frac{\Delta t^5}{1920}(u_{ttttt})_{0,0}^{j}$ in eq. (A1).